

Spontaneous deformation and fission of oil droplets on an aqueous surfactant solution

Masahide Okada,¹ Yutaka Sumino,^{2,3} Hiroaki Ito,¹ and Hiroyuki Kitahata^{1,*}

¹*Department of Physics, Chiba University, Chiba 263-8522, Japan*

²*Department of Applied Physics, Tokyo University of Science, Tokyo 125-8585, Japan*

³*W-FST, I² Plus, and DCIS, RIST, Tokyo University of Science,*

6-3-1 Nijuku, Katsushika-ku, Tokyo, 125-8585, Japan

(Dated: June 12, 2025)

We investigated the spontaneous deformation and fission of a tetradecane droplet containing palmitic acid (PA) on a stearyltrimethylammonium chloride (STAC) aqueous solution. In this system, the generation and rupture of the gel layer composed of PA and STAC induce the droplet deformation and fission. To investigate the characteristics of the droplet-fission dynamics, we obtained the time series of the number of the droplets, and confirmed that the number has a peak at a certain STAC concentration. Since the fission of the droplet should be led by the deformation, we analyzed four parameters which may relate to the fission dynamics from the spatio-temporal correlation of the droplet-boundary velocity. As a result, we found that the faster deformation would be the key factor for the fission dynamics.

I. INTRODUCTION

Self-propelled objects have been intensively studied as examples of nonequilibrium systems. These objects move through the transduction of chemical energy to mechanical energy. For example, alcohol droplets[1–3] and camphor disks[4, 5] on an aqueous phase, alcohol droplets on an oil phase[6], soap disks at an oil-water interface[7, 8], aqueous droplets with a periodic chemical reaction[9, 10], and oil droplets in a surfactant aqueous solution[11–13] are typical self-propelled objects. They are driven by the surface-tension gradient originating from the concentration gradient of the chemicals. In the case that the driving force overcomes the interfacial tension that tends to keep the droplet shape spherical, they exhibit shape deformation as well as motion.

Through dynamic deformation, the liquid droplets can also exhibit fission[1, 2, 6, 9–12]. Nagai et al. reported the spontaneous motion, deformation, and fission of a pentanol droplet on a water surface, and performed the stability analyses[1]. Keiser et al. discussed the spread and successive fragmentation at the periphery of an alcohol-aqueous-solution droplet on an oil phase based on the experimental results and scaling analyses[6]. In these systems, once the periphery of the alcohol droplet is rippled, such deformation grows due to the instability induced by the interfacial-tension gradient and finally leads to the droplet fission. Many other studies have also reported the droplet fission due to the Marangoni effect[2, 9–12, 14].

It was reported that a tetradecane droplet containing palmitic acid (PA) on an aqueous solution of stearyltrimethylammonium chloride (STAC) exhibits spontaneous blebbing and fission[15, 16]. The blebbing means the formation of bleb, spherical deformation, which resembles the one observed in cell deformation[17].

It is suggested that the blebbing observed in the PA-STAC system is caused by the formation of the gel-layer with lamellar structures composed of PA and STAC, which was confirmed by time-dependent small-angle X-ray scattering (SAXS)[18, 19]. The formation of the gel layer increases the inner pressure of the oil droplet. The fragile part expands in a circular shape owing to the increased inner pressure, and eventually the gel layer is ruptured. Then the oil phase touches the aqueous phase, and the expanded part shrinks by the interfacial tension between the oil and the aqueous phases. As the result of the blebbing, the oil droplet sometimes exhibits fission. It should be noted that the typical timescale of the oil droplet fission led by the blebbing $\sim 10^1$ – 10^3 s is longer than that led by Marangoni effect $\sim 10^0$ – 10^1 s in the systems with the lengthscale of mm. Detailed analyses of the droplet deformation focusing on the surface velocity were performed and it was confirmed that the droplet exhibits blebbing irregularly, that is to say, neither long-range spatial correlation nor long-time temporal correlation was observed[20]. The surfactant-concentration dependence of the droplet blebbing was also studied, and the droplet behaviors were classified into the three types depending on the concentrations: fission induced by interfacial blebbing, interfacial blebbing without fission, and the formation of the white-turbid aggregate that covers the droplet[21].

In the present study, we report the details of the oil droplet fission caused by the generation and rupture of the gel layer in the same system as the previous studies[15, 18–21]. We experimentally obtained the time series of the number of the droplets for various STAC concentrations. To discuss the fission dynamics, we investigated the dynamics of the droplet deformation for various STAC concentrations and extracted four characteristic parameters which seem to relate with the mechanism of fission from the droplet-deformation dynamics. From these investigations, we revealed the relationship between deformation and fission, and found the key parameter that may affect the droplet fission.

* kitahata@chiba-u.jp

II. EXPERIMENTAL SETUP

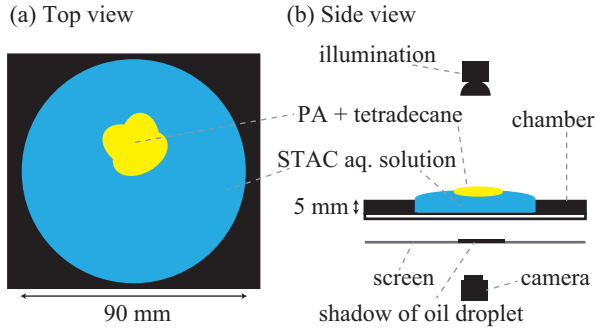


FIG. 1. Experimental setup. (a) Top view. (b) Side view. The chamber was made of a teflon plate with a circular hole (diameter: 90 mm, thickness: 5 mm) attached to an acrylic plate. The chamber was filled with STAC aqueous solution with a volume of 38 ml. An oil droplet with a volume of 0.8 ml was put on the surface of the STAC solution.

STAC and PA were purchased from Tokyo Chemical Industry Co., Ltd., Tokyo, Japan. Tetradecane was purchased from Sigma-Aldrich, St. Louis, USA. Water was purified by Elix UV 3 (Merck, Darmstadt, Germany). We prepared a teflon plate with a circular hole (diameter: 90 mm, thickness: 5 mm) attached to an acrylic plate, which was used as a chamber. Experimental setup is schematically illustrated in Fig. 1. The chamber was filled with 38 ml of STAC aqueous solution, and 0.8 ml of PA tetradecane solution was put as a droplet on the aqueous surface. The concentration of STAC, C , was varied from 0.2 to 5 mM, while the concentration of PA was fixed at 20 mM. In this condition, it was reported that the droplets deform and exhibit fission[21].

We put a tracing paper as a screen under the chamber and illuminated the oil droplet from the top. We recorded the shadow of the droplet on the screen from the bottom using a USB camera (DMK 24UJ003; Imaging Source Asia Co., Ltd., Taipei, Taiwan) at 1 fps. All experiments were carried out at room temperature ($23.5 \pm 1.5^\circ\text{C}$).

III. EXPERIMENTAL RESULTS

After putting the oil droplet on the aqueous phase, it had a circular shape during an induction period (~ 10 s)[15]. After the induction period, the oil droplet suddenly exhibited quick spread and shrinkage within a few seconds. After these behaviors, blebbing started, where the droplet boundaries exhibited slow circular expansion followed by rapid shrinkage in a spatio-temporally random manner[15]. As a result of the successive blebbing, the oil droplet sometimes exhibited fission. After several ten minutes, the fission ceased eventually.

The snapshots of the droplets for various C are shown in Fig. 2(a). For the oil droplets with $C = 0.2$ mM, they

sometimes exhibited fission with the larger deformation by frequent blebbing. The oil droplets with $C = 2$ mM frequently exhibited fission associated with the frequent smaller blebbing. The oil droplets with $C = 5$ mM exhibited fission less frequently compared to the ones with $C = 2$ mM, and had circular shapes with small blebbing. We obtained ensemble data through 10 trials to evaluate the behaviors of the oil droplets and to confirm the reproducibility. The mean number of droplets, $\langle N(t) \rangle$, and the individual data are shown with a thick line and thin lines, respectively, in Fig. 2(b).

Figure 3(a) shows $\langle N(t) \rangle$ for various C . For $C = 0.2$ –2 mM, $\langle N(t) \rangle$ rapidly increased during the first 1000 s, and then converged to each final value depending on C . On the other hand, for $C = 3$ –5 mM, $\langle N(t) \rangle$ slowly increased during the first 1000 s, then started rapid increases, and finally converged to each final value. Figure 3(b) shows the final number of the droplets N_{fin} versus C . For the lower concentrations $C = 0.2$ –2 mM, N_{fin} increased with an increase in C . For the higher concentrations $C = 2$ –5 mM, in contrast, N_{fin} decreased with an increase in C . In other words, N_{fin} had a peak at $C = 2$ mM.

IV. DISCUSSION

In our experimental results, N_{fin} has a peak at $C = 2$ mM as shown in Fig. 3(b). To discuss the underlying mechanism for the concentration dependence, we investigated the deformation of the oil droplets because our experimental observation suggests the correlation between deformation and fission.

Here, we analyzed the concentration-dependent deformation observed in experiments equivalent to those in Sec. III except for the time resolution. The initial deformation just after the induction period was captured at 30 fps, and the captured images were processed as follows. First, we binarized the images to extract the droplet region, and set the polar coordinates (r, θ) , where the origin was at the center of mass of the droplet as shown in Fig. 4(a). In these coordinates, we detected the boundary of the droplet $r(\theta, t)$ at $\theta = \theta_n$ and $t = t_m$. Here, $\theta_n = 2\pi n/N_\theta$ rad ($n = 0, 1, \dots, N_\theta - 1$) and $t_m = m/30$ s ($m = 0, 1, \dots, N_t - 1$), where $N_\theta = 1024$ and $N_t = 1024$. We calculated the boundary velocity $v(\theta, t)$ also at $\theta = \theta_n$ and $t = t_m$ from the time difference of $r(\theta, t)$, and plotted the spatio-temporal map of $v(\theta, t)$ in the same manner as the previous study[20] in Fig. 4(b). Figure 4(c) is the magnification of the region in the yellow dashed rectangle in Fig. 4(b), which corresponds to a single cycle of the expansion and shrinkage, i.e., a single blebbing dynamics. As a typical blebbing dynamics, the arc length of the boundary with a positive outward velocity increases, and a bright triangular region appears in the spatio-temporal map. Note that the brighter triangular shape suggests that the edges of the blebbing region are not pinned but they expand with

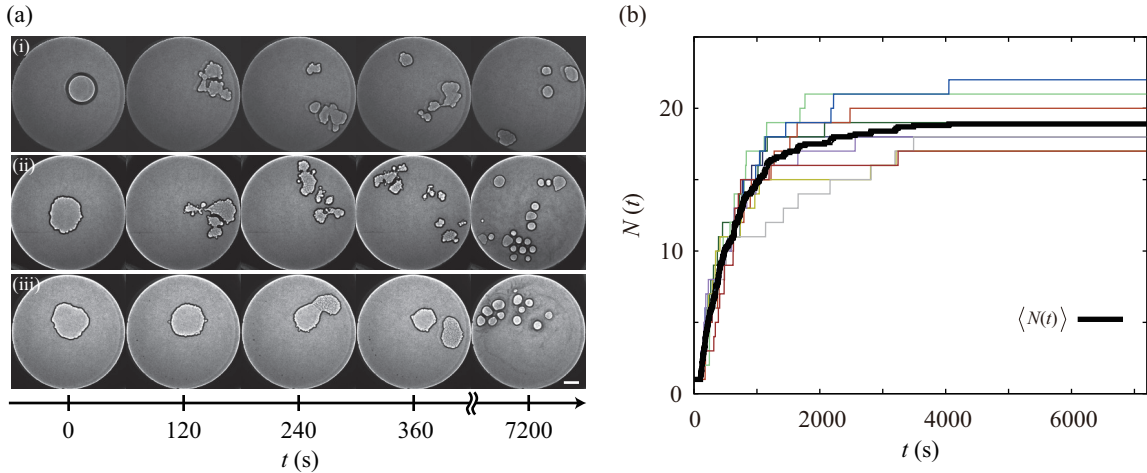


FIG. 2. Experimental results on the droplet fission. (a) Snapshots for various C . Scale bar: 10 mm. (i) 0.2 mM (ii) 2 mM (iii) 5 mM. (b) Time series of the number of the oil droplets for $C = 2$ mM. The thin lines show the experimental results for 10 trials, and the thick line shows the mean value.

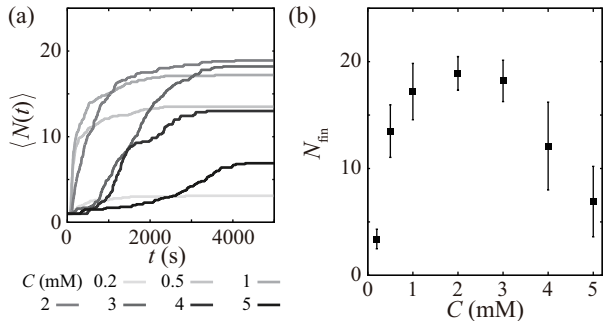


FIG. 3. The number of droplets for various C . (a) Time series of the average number of oil droplets, $\langle N(t) \rangle$, for various C . (b) The final number of oil droplets, N_{fin} , for various C . N_{fin} has a peak at $C = 2$ mM. Error bars represent standard deviations.

time as shown in Fig. 4(d). In other words, the bleb expands almost in a circular manner. After the expansion, the expanded part shrinks rapidly and a dark thin region appears in the map. Meanwhile, the maximum lengths of the triangular regions along a horizontal axis correspond to the maximum bleb size measured with the angle. The maximum lengths of bright and dark regions along a vertical axis represent the timescale of expansion and shrinkage, respectively. For the entire droplet deformation, a lot of similar patterns are incoherently distributed as seen in Fig. 4(b), which is consistent with the previous report[20].

We calculated the auto-correlation function $g(\Delta\theta) = \langle v(\theta, t)v(\theta + \Delta\theta, t) \rangle_{\theta, t}$ as shown in Fig. 5(a), where $\Delta\theta$ represents angle difference and $\langle \cdot \rangle_{\theta, t}$ represents the average over θ and t . The correlation angle θ_c was defined as the smallest $\Delta\theta$ that satisfied $g(\Delta\theta) = 0$. Figure 5(b) shows the C dependence of the correlation angle θ_c . θ_c decreased with an increase in C .

We estimated the typical timescale of deformation. Only when the droplet shape changes far from circular, the droplet can exhibit fission. For such large deformation, expansion is necessary rather than shrinkage. Thus, we consider that the droplet-boundary expansion would provide the essential information for the droplet fission. The timescale of expansion was longer than that of shrinkage as we can see the longer vertical length of the bright region than that of the dark region (Fig. 4(c)). We supposed that we can extract the two timescales from the time-domain auto-correlation function, but it was difficult to distinguish them (see Appendix A). To evaluate the characteristic timescale of expansion t_c , we applied two-dimensional fast Fourier transform (FFT) to $v(\theta, t)$. Figure 6(a) shows the typical result of the two-dimensional FFT, in which the horizontal axis corresponds to the angular wavenumber k , and the vertical axis to the angular frequency ω . From the characteristic triangular patterns seen in $v(r, \theta)$ map (Fig. 4(c)), we can see that the droplet boundaries expand at a constant rate. In the FFT image, the bright lines orthogonal to the original triangular patterns should appear; We can see two white inclined lines and a white vertical band in Fig. 6(a). The inclined lines with the slope of α correspond to the triangular bright regions in Fig. 4(c). Notably, α corresponds to the expansion rate of the central angle of the bleb. The white vertical band corresponds to the almost horizontal patterns of the thin dark regions in the original spatio-temporal map. The detailed explanations for extracting the correlation time from the FFT image are described in Appendix B.

Figure 6(b) shows the C dependence of the expansion rate α . For $C < 2$ mM, α increased with an increase in C . For $C > 2$ mM, α slightly decreased with an increase in C but was kept almost constant at $\alpha \approx 0.06$ rad/s. We calculated the characteristic timescale of expansion t_c as $t_c = \theta_c/\alpha$. Figure 6(c) shows the C dependence

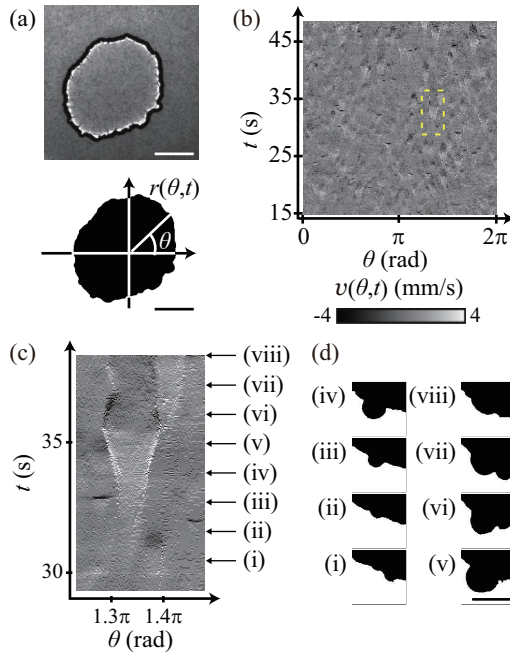


FIG. 4. Dynamics of the droplet deformation for $C = 4$ mM. (a) Binarization of the droplet image and definition of the polar coordinates. Scale bar: 10 mm. The center of mass of the droplet was set to be the origin. (b) Spatio-temporal map of the boundary velocity $v(\theta, t)$. (c) Magnification of the region in the yellow dashed rectangle in (b). (d) Snapshots of the binarized images of a single blebbing dynamics corresponding to (c) every 1 s. Scale bar: 5 mm.

of t_c . Qualitatively similar to the C dependence of θ_c , t_c decreased with an increase in C . The bleb size V was calculated as $V = R^2 \theta_c t_c \alpha$, and its C dependence is shown in Fig. 6(d). To obtain the bleb size V , we assumed the concentric-circle-like expansion. The average radius of the droplet R was estimated by $R = \sqrt{S/\pi}$, where S is the droplet area, and we found it almost constant at $R \approx 12$ mm from the experiments. V also decreased with an increase in C . Then, we calculated the correlation coefficients between N_{fin} and one of the parameters θ_c , α , t_c , and V from their C dependence, as shown in Fig. 7. From this result, we confirmed that the absolute value of the correlation coefficient between N_{fin} and α was the largest. It should be noted that the sign of the correlation coefficient was positive for α and negative for the others. Considering the strongest positive correlation between α and N_{fin} , the high expansion rate would most strongly contribute to the frequent fission. It seems that the discussion of kinetic process is important rather than the geometric information of the blebbing to understand the mechanism of the fission.

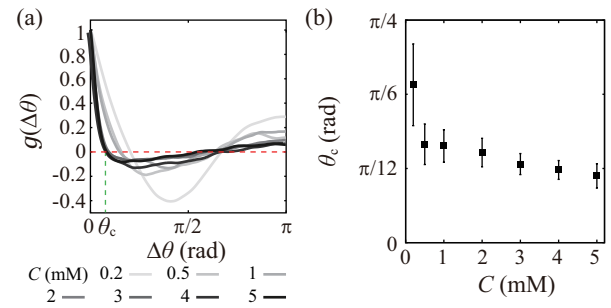


FIG. 5. (a) Autocorrelation function, $g(\Delta\theta)$, of the boundary velocity $v(\theta, t)$ for various C . See the main text for the detailed definition of $g(\Delta\theta)$. Here, the correlation angle θ_c was defined as the smallest $\Delta\theta$ that satisfies $g(\Delta\theta) = 0$. (b) θ_c versus C . Error bars represent standard deviations.

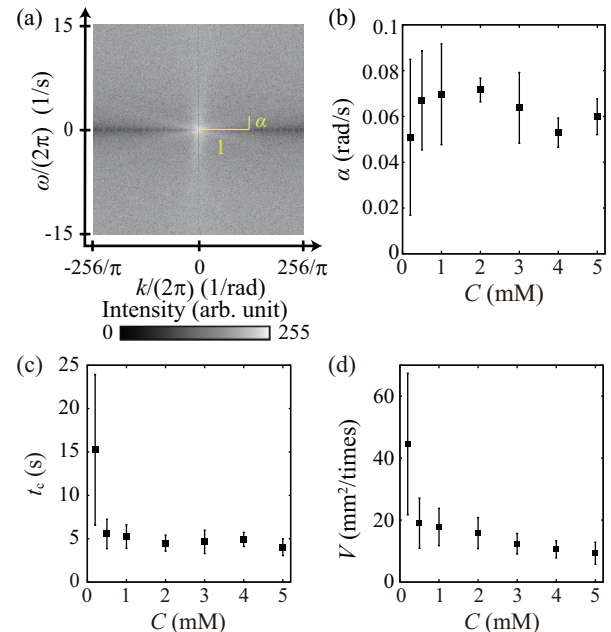


FIG. 6. Dynamics of the droplet deformation. (a) FFT image of Fig. 4(b). Two white inclined lines crossing at the origin correspond to the boundary expansion of the droplet. We measured the slope α of the white lines. The almost vertical line corresponds to the rapid shrinkage. (b) Expansion rate α versus C . (c) Characteristic timescale of expansion t_c versus C . (d) Bleb size V versus C . Error bars represent standard deviations.

V. CONCLUSION

We studied the fission of the tetradecane droplet containing PA on the STAC aqueous solution for various STAC concentrations. The number of the oil droplets at the final stage of the observation had a peak at a certain concentration. To discuss the droplet fission dynamics, we extracted the boundary velocity from the time series of the droplet deformation and calculated the correlation in time and space for various STAC concentrations.

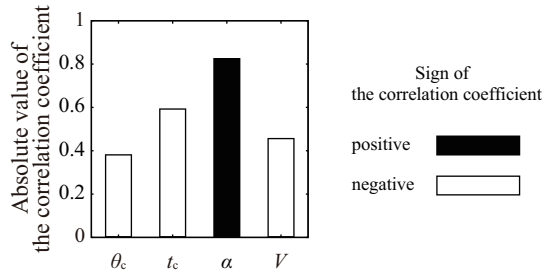


FIG. 7. Absolute values of the correlation coefficients between the final number of the oil droplets N_{fin} and one of the four parameters: correlation angle θ_c , characteristic timescale of expansion t_c , expansion rate of the central angle of the bleb α , and blebbing volume V . Filled and open bars represent positive and negative correlations, respectively.

We obtained the four parameters that characterize the droplet deformation: the correlation angle, the characteristic timescale of expansion, the expansion rate, and the bleb size. Among them, the expansion rate had the strongest positive correlation with the final number of the droplets, and therefore it is suggested that faster deformation leads more frequent fission. It is known that the generation and rupture of the active gel are also seen in the migration, deformation and fission of living cells[22–25]. The present results might also help understand such phenomena by considering the common features.

ACKNOWLEDGMENTS

This work was supported by JSPS KAKENHI Grant Numbers JP19H00749, JP19H05403, JP19K14675, JP16H03949. It was also supported by Sumitomo Foundation (No. 181161), the Japan-Poland Research Co-operative Program “Spatio-temporal patterns of elements driven by self-generated, geometrically constrained flows”, and the Cooperative Research Program of “Network Joint Research Center for Materials and Devices” (No. 20191030).

Appendix A: Time-domain auto-correlation function

We obtained the time-domain auto-correlation function $h(\Delta t) = \langle v(\theta, t)v(\theta, t + \Delta t) \rangle_{\theta, t}$ shown in Fig. 8(a). $h(\Delta t)$ for each C became negative where $\Delta t = 1/30$ s, the minimum time interval, because $h(\Delta t)$ is calculated from the boundary velocity calculated from the time difference of the boundary position with pixel noises. That is to say, the velocities at two time points with the minimum time interval tend to have the negative correlation by such pixel noises. Therefore we detected the second smallest Δt at which $h(\Delta t)$ crosses 0 from positive to negative. This Δt , represented as t_{cs} , is a candidate for the characteristic timescale of the expansion, which is plotted in Fig. 8(b) for each C . The typical order of t_{cs} is

the same as t_c shown in Fig. 6(c). However, there should be two significant timescales in the blebbing deformation: those of expansion and shrinkage. It was difficult to judge whether t_{cs} corresponds to the timescale of expansion, as we could not find any remarkable feature for the two different timescales greater than 1/30 s in Fig. 8(a). This is the reason why we did not use $h(\Delta t)$ to analysis the timescale of expansion.

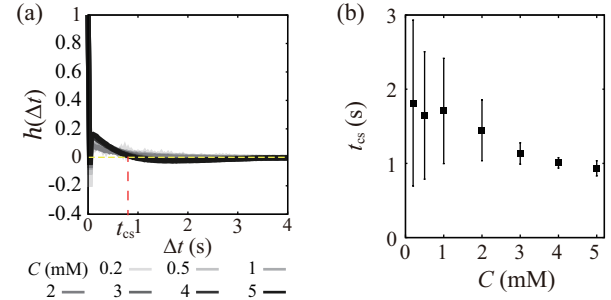


FIG. 8. (a) Time-domain auto-correlation function, $h(\Delta t)$, of the boundary velocity $v(\theta, t)$ for various C . Detailed definition of $h(\Delta t)$ is in the text. The second smallest Δt at which $h(\Delta t)$ crosses 0 from positive to negative is set as t_{cs} . (b) t_{cs} versus C . Error bars represent standard deviations.

Appendix B: FFT image of spatio-temporal map

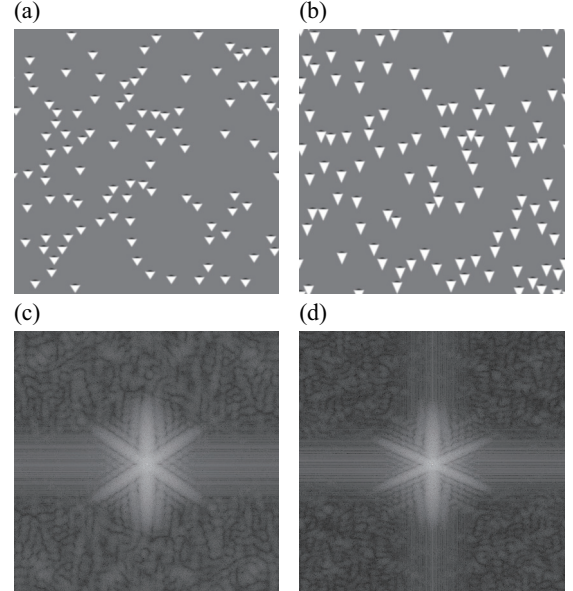


FIG. 9. Demonstrative FFT analyses with artificially generated images. (a,b) Artificially generated spatio-temporal maps with different lengths of the white regions along a vertical axis, which correspond to the analysis of the droplet deformation in Fig. 4(b). Detailed setup of these maps are written in the text. (c,d) FFT images of (a,b), respectively.

We demonstrate the correspondence of the two-dimensional patterns in the spatio-temporal map and those in the FFT image shown in Figs. 4(b) and 6(a). Figure 9(a) and 9(b) are the artificially generated spatio-temporal maps that correspond to the random deformation of the droplet boundary without noise. The lengths of white regions along a vertical axis in Figs. 9(a) and 9(b) are 35 and 45 pixels, respectively. The difference in the length along a vertical axis corresponds to that in the timescale of expansion. The gray region represents stationary boundary, the white ones represent boundary expansion, and the black ones represent boundary shrinkage. A pair of white and black regions corresponds to a single blebbing and is called a blebbing area. In these maps, 100 blebbing areas are scattered in a spatio-temporally random manner. Gaussian blur with the standard deviation of 2 pixels is applied to the both of 1024×1024 images. Figures 9(c) and 9(d) correspond to

the FFT images of Figs. 9(a) and 9(b), respectively. In both of these images, a vertical white line and two inclined white lines can be seen. As indicated in Fig. 9(c) and 9(d), the different lengths of the white region along the vertical axis result in the different slopes of the two inclined lines, referred to as α . Thus, the two inclined lines correspond to the structure factor of the white regions.

In the FFT images, we can also find a white vertical band as seen in the experimental data in Fig. 6(a). In the analyses of the experimental data, we subtracted the translational motion of the droplet. It corresponds to the removal of the spatial first mode (± 1 mode) of the FFT images, which can be observed as the two vertical black thin lines in Fig. 6(a). Because the artificially generated spatio-temporal maps in Figs. 9(a,b) include the first mode, such two vertical black lines are absent in Figs. 9(c,d).

[1] K. Nagai, Y. Sumino, H. Kitahata, and K. Yoshikawa, *Phys. Rev. E* **71**, 065301 (2005).

[2] K. H. Nagai, K. Tachibana, Y. Tobe, M. Kazama, H. Kitahata, S. Omata, and M. Nagayama, *J. Chem. Phys.* **144**, 114707 (2016).

[3] N. J. Cira, A. Benusiglio, and M. Prakash, *Nature* **519**, 446 (2015).

[4] S. Nakata, Y. Iguchi, S. Ose, M. Kuboyama, T. Ishii, and K. Yoshikawa, *Langmuir* **13**, 4455 (1997).

[5] M. I. Kohira, Y. Hayashima, M. Nagayama, and S. Nakata, *Langmuir* **17**, 7124 (2001).

[6] L. Keiser, H. Bense, P. Colinet, J. Bico, and E. Reyssat, *Phys. Rev. Lett.* **118**, 074504 (2017).

[7] S. Nakata and S. Hiromatsu, *Chem. Phys. Lett.* **405**, 39 (2005).

[8] F. Takabatake, N. Magome, M. Ichikawa, and K. Yoshikawa, *J. Chem. Phys.* **134**, 114704 (2011).

[9] H. Kitahata, N. Yoshinaga, K. H. Nagai, and Y. Sumino, *Chem. Lett.* **41**, 1052 (2012).

[10] I. Derényi and I. Lagzi, *Chem. Phys. Phys. Chem.* **16**, 4639 (2014).

[11] V. Pimienta, M. Brost, N. Kovalchuk, S. Bresch, and O. Steinbock, *Angew. Chem. Int. Ed.* **50**, 10728 (2011).

[12] F. Caschera, S. Rasmussen, and M. M. Hanczyc, *ChemPhysChem* **78**, 52 (2013).

[13] M. M. Hanczyc, T. Toyota, T. Ikegami, N. Packard, and T. Sugawara, *J. Am. Chem. Soc.* **129**, 9386 (2007).

[14] U. Brosa and S. Grossmann, *Phys. Lett. B* **126**, 425 (1983).

[15] Y. Sumino, H. Kitahata, H. Seto, and K. Yoshikawa, *Phys. Rev. E* **76**, 055202 (2007).

[16] Y. Sumino, in *Self-organized motion: Physicochemical design based on nonlinear dynamics*, eds. S. Nakata, V. Pimienta, I. Lagzi, H. Kitahata, and N. J. Suematsu (R. Soc. Chem., Cambridge, 2019).

[17] G. T. Charras, *J. Microsc.* **231**, 466 (2008).

[18] Y. Sumino, H. Kitahata, Y. Shinohara, N. L. Yamada, and H. Seto, *Langmuir* **28**, 3378 (2012).

[19] Y. Sumino, N. L. Yamada, M. Nagao, T. Honda, H. Kitahata, Y. B. Melnichenko, and H. Seto, *Langmuir* **32**, 2891 (2016).

[20] Y. Sumino, H. Kitahata, H. Seto, and K. Yoshikawa, *Soft Matter* **7**, 3204 (2011).

[21] Y. Sumino, H. Kitahata, H. Seto, S. Nakata, and K. Yoshikawa, *J. Phys. Chem. B* **113**, 15711 (2009).

[22] T. J. Mitchison and L. P. Cramer, *Cell* **84**, 371 (1996).

[23] J. Condeelis, *Trends Cell Biol.* **3**, 371 (1993).

[24] G. T. Charras, J. C. Yarrow, M. A. Horton, L. Mahadevan, and T. J. Mitchison, *Nature* **435**, 365 (2005).

[25] J. Prost, F. Jülicher, and J-F. Joanny, *Nat. Phys.* **11**, 111 (2015).